Original Article

Institution of MECHANICAL ENGINEERS
Journal of MATERIALS: DESIGN AND APPLICATIONS

Proc IMechE Part L:
J Materials: Design and Applications
2015, Vol. 229(5) 380–388

DOI: 10.1177/1464420714524930
pil.sagepub.com
SAGE

Towards square hole-flanging produced by single point incremental forming

VAM Cristino[1], L Montanari[2], MB Silva[3] and PAF Martins[3]

Abstract

This paper presents the first investigation on square hole-flanging produced by single point incremental forming. The aim and objective is to provide readers with a broad understanding on the deformation mechanics of the process that will enable them to understand plastic flow resulting from the interaction between the tool and the blank, to identify the influence of the pre-cut geometry in the overall formability, and to characterize the physics of failure. The methodology comprises the mechanical characterization of the material, the use of circle grid analysis, and the fabrication of square flanges with round corners by multistage single point incremental forming using blanks with different pre-cut hole geometries. The investigation is performed in aluminium AA1050-H111 and the overall results widens and enhances current research work in hole-flanging of cylindrical parts by giving the first contribution towards the understanding of plastic flow and failure in hole-flanging of square parts produced by single point incremental forming.

Keywords

Single point incremental forming, square hole-flanging, deformation, formability, fracture

Date received: 18 September 2013; accepted: 30 January 2014

Introduction

Single point incremental forming (SPIF) is an emerging dieless manufacturing process in which a simple forming tool, whose path is generated in a computer-aided manufacturing (CAM) software and fed in a computer numerical controlled (CNC) machining center, is utilized to shape a blank into a sheet forming component. The basic components of SPIF are schematically illustrated in Figure 1(a) and comprise: (i) the blank, (ii) the rig with the backing plate (not seen in the figure), (iii) the pressure pad, and (iv) the single point forming tool. The periphery of the blank is placed on top of the backing plate and is rigidly clamped around its edges by the pressure pad. The remaining surface of the blank is unsupported underneath and is progressively shaped by a free (or rotating) hemispherical-ended forming tool that describes the contour of the final desired geometry. The state-of-the-art and potential applications of SPIF are comprehensively described in the state-of-the-art review papers by Jeswiet et al.[1] and Nimbalkar and Nandedkar.[2]

Hole-flanging produced by SPIF is a recent variant in which a blank with a pre-cut hole is progressively shaped with a single point forming tool to fabricate flanges that may be used to reinforce the edge of the holes, to enhance its shape and to attach tubes or profiles to sheets. The process was originally developed by Cui and Gao[3] in 2010 as an alternative to conventional hole-flanging produced by press-working for rapid prototyping and flexible small-batch production.

Over the past three years hole-flanging produced by SPIF has been investigated by several other researchers. Petek et al.[4] studied the influence of multistage backward tool paths in the overall formability of the process. Centeno et al.[5] characterized the deformation mechanics of the process and the physics behind the occurrence of failure. Montanari et al.[6] determined the experimental distribution of strains and stresses and presented the results in the principal strain and stress spaces. Silva et al.[7] extended the domain of application of hole-flanging produced by SPIF to commercial polymer blanks, at room temperature.

Despite the growing research interest on hole-flanging produced by SPIF, the existing publications are primarily and almost exclusively focused on

[1]Department of Electromechanical Engineering, University of Macau, Macau, China
[2]Escola de Engenharia de São Carlos, University of São Paulo, São Carlos, Brazil
[3]Instituto Superior Tecnico, Universidade de Lisboa, Lisboa, Portugal

Corresponding author:
PAF Martins, Instituto Superior Tecnico, Universidade de Lisboa, Av. Rovisco Pais, 1049-001, Lisboa, Portugal.
Email: pmartins@ist.utl.pt

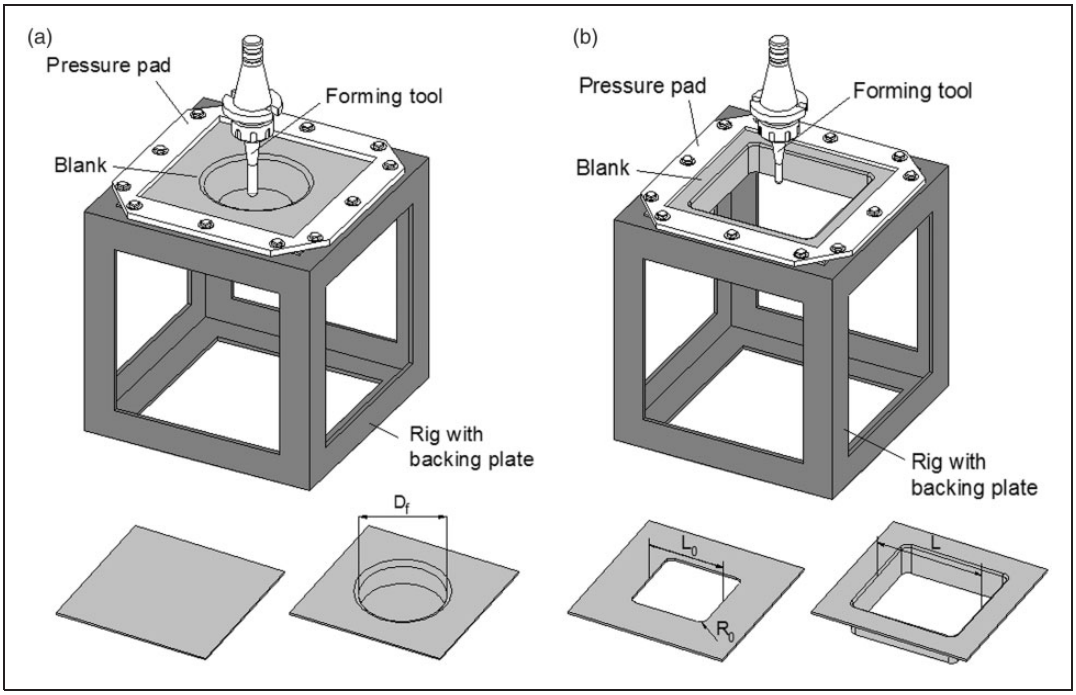

Figure 1. Schematic representation of the single point incremental forming (SPIF) process: (a) experimental layout, detail of the initial blank and corresponding cylindrical cup produced by (axisymmetric) SPIF; (b) experimental layout, detail of the initial blank with a pre-cut hole and corresponding square flange with round corner produced by (asymmetric) SPIF.

conical and cylindrical flanges obtained from blanks with pre-cut circular holes. The only two exceptions, as far as the authors are aware, are the publications authored by Petek et al.[4] and Voswinckel et al.[8]

Petek et al.[4] showed that asymmetrical round flanges can also be produced by SPIF but claimed that significant trial-and-error procedures had to be made in order to produce the required flanges. They attributed the cause of this to inappropriate definition of the initial shape of the pre-cut hole and to different deformation history along the wall, and concluded that research in hole-flanging produced by SPIF should be directed towards the challenge of producing asymmetrical hole-flanges with minimal trial-and-error procedures. Voswinckel et al.[8] investigated the feasibility of fabricating stretch and shrink flanges at the sheet edges by multistage SPIF. They studied the influence of tool path strategies and concluded that the feasibility ratios of flange length to flange radii could distinctively exceed those of conventional flanging produced by press-working.

From what was mentioned before, it can be concluded that there is a need to perform a phenomenological study of asymmetric hole-flanging produced by SPIF focused on plastic flow and failure. This paper is intended to meet this objective by resorting to square flanges with round corners (Figure 1(b)) as a means of achieving a broader understanding of the deformation mechanics of complex asymmetric hole-flanging produced by SPIF. The overall strategy involves breaking down the square flanges into different regions containing the corners, the walls and the transition between the corners and the walls that are commonly found in square hole-flanges.

Under these circumstances, this paper should be considered as the first investigation towards the understanding of plastic flow and failure in square hole-flanging produced by SPIF that aims to give answers to the following main questions: What is the influence of the pre-cut hole geometry in the overall formability of the process? Which are the main differences in plastic flow arising from the interaction between the forming tool and the blank in different locations of the parts? Which is the physics of failure in square hole-flanging? What is the feasibility of setting-up the process window as a function of the main operating parameters?

The answer to these questions is given by means of an experimental-based investigation that combines circle grid analysis, mechanical characterization of the material, and fabrication of square flanges with round corners by multistage SPIF.

Material and methods

Mechanical and formability characterization

The research work was carried out on aluminium AA1050-H111 sheets with 1 mm thickness. Tensile tests performed in specimens cut out from the sheets at 0°, 45°, and 90° with respect to sheet rolling direction allowed determining the modulus of elasticity E, the yield strength σ_Y, the ultimate tensile strength σ_{UTS}, the anisotropy coefficient r, and the elongation

Table 1. Mechanical properties of the aluminium AA1050-H111 sheets.

	Modulus of elasticity, E (GPa)	Yield strength, σ_Y (MPa)	Ultimate tensile strength, σ_{UTS} (MPa)	Anisotropy coefficient, r	Elongation at break, A (%)
0° RD	72.7	115.4	119.0	0.71	7.1
45° RD	67.9	120.4	121.2	0.88	5.2
90° RD	71.8	123.0	120.8	0.87	5.6
Average	70.0	119.9	120.5	0.84	6.8

at break A (refer to Table 1). The average value of the anisotropy coefficient $\bar{r}$ was obtained from

$$\bar{r} = \frac{r_0 + 2r_{45} + r_{90}}{4} \quad (1)$$

The average stress–strain curve resulting from the tensile tests was approximated by the following Ludwik–Hollomon's equation

$$\sigma = 140\varepsilon^{0.04}(\text{Mpa}) \quad (2)$$

The formability limits at the onset of necking (hereafter referred to as "the forming limit curve" or simply as "FLC") and the formability limits at fracture (hereafter referred to as "the fracture forming line" or simply as "FFL") were characterized by means of sheet metal formability tests that covered strain paths from uniaxial to plane-strain and biaxial loading conditions. The specimens utilized in the tests were cut out from the supplied sheets by means of a blanking tool and subsequently abraded with sand papers (with grades 400, 600, and 800) to eliminate burrs, cracks and to smooth and make the edges perpendicular to the surface of the sheets. The procedure utilized to determine the in-plane strains (ε_1, ε_2) of the specimens made use of overlapping circle grids with 2 mm initial diameter d that were imprinted by electrochemical etching. The measurements of the major a and minor b axes of the ellipses that resulted from plastic deformation were carried out by a computer-aided measuring system (CAMS) (Figure 2(a)) and the resulting in-plane strains (ε_1, ε_2) were calculated as follows

$$\varepsilon_1 = \ln\left(\frac{a}{d}\right) \quad \varepsilon_2 = \ln\left(\frac{b}{d}\right) \quad (3)$$

The FLC was obtained by determining the principal strains (ε_1, ε_2) at failure from the grid points adjacent to the neck because they represent the uniform thinned sheet condition at the onset of necking. In practical terms, authors made use of Zurich No. 5 experimental procedure for determining the strains at necking by means of the strains retrieved from measurements in adjacent deformed circles along a direction perpendicular to the crack.

The FFL cannot be determined from the grid points located in the necking region close to fracture because, no matter how small the circles are, the resulting principal strains can never be taken as the fracture strains. Instead, the FFL was obtained by determining the "gage length" strains resulting from thickness measurements along the crack. The strain values at fracture were then fitted by a line falling from tension–compression to tension–tension in accordance to the condition of critical thickness reduction[9]

$$\varepsilon_1 + 0.68\varepsilon_2 = 1.34 \quad (4)$$

The resulting formability limits at necking (FLC) and fracture (FFL) are plotted in Figure 2(b) and the bounded grey area around the FFL corresponds to an interval of 10% due to the uncertainty in its determination. Further details on the experimental techniques that were employed to determine the FLC and the FFL can be found in Silva et al.[10]

Hole-flanging experiments

The experiments were carried out in a Deckel Maho CNC machining centre equipped with a rig (refer to Figure 1(b)). The plan of experiments was aimed at investigating the influence of the pre-cut hole geometry on plastic flow and fracture of square flanges with round corners fabricated by multistage SPIF. The thickness t_0 of the blanks, the initial drawing angle ψ_1 and the tool diameter, step size and feed rate were kept constant because they were already investigated in conventional SPIF[11,12] and cylindrical hole-flanging produced by SPIF.[3,5] This allowed focus to be placed on the design of the pre-cut holes and on the understanding of the deformation mechanics along the inclined flange walls.

The abovementioned strategy copes with the need to investigate the initial shape of the pre-cut holes and the deformation history along the flange walls that was previously identified by Petek et al.[4] after performing a significant amount of trial-and-error

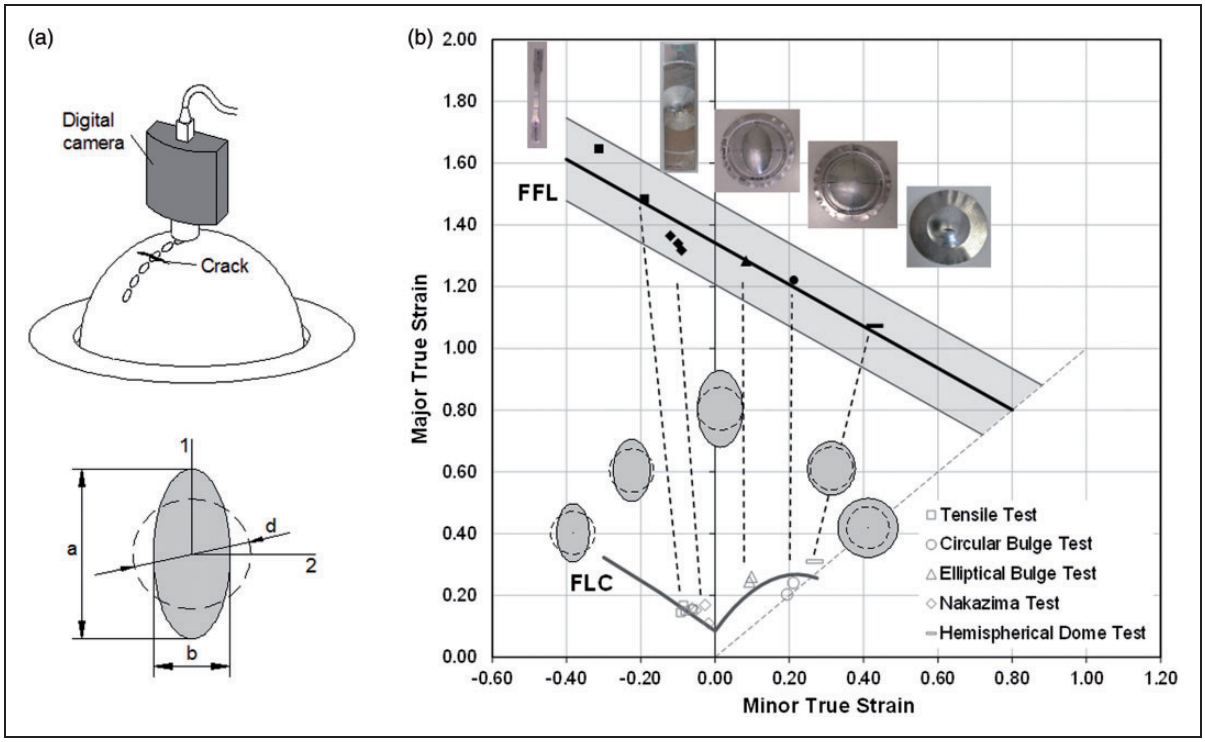

Figure 2. Experimental determination of the formability limits of aluminium AA1050-H111: (a) schematic representation of the procedure that was utilized for measuring the major and minor in-plane strains from the grids; (b) forming limit curve (FLC) and fracture forming line (FFL) in the principal strain space (forming limit diagram). The solid markers refer to failure by fracture and the black dashed lines show the change in strain path direction towards plane strain after necking.

procedures to obtain sound asymmetrical round flanges produced by SPIF.

The aluminium AA1050-H111 initial blanks with 250 mm × 250 mm × 1 mm were milled to deliver square pre-cut holes with different side lengths L_0 and corner radii R_0. The hole edges were subsequently ground with grit sand paper to eliminate burrs, cracks and to make the edges perpendicular to the surfaces. After being ground, the blanks were electrochemically etched with grids of overlapping circles with 2 mm initial diameter in order to allow in-plane strains to be measured from the deformed ellipses.

The flanges were shaped by means of a multistage forward tool path strategy that made use of progressively increasing drawing angles from $\Psi_1 = 65^\circ$, until $\Psi_6 = 90^\circ$ with steps of $\Delta\Psi = 5^\circ$ in order to obtain vertical walls with 170 mm side length L. The forming tool had a hemispherical tip with 8 mm diameter and was made from cold working 120WV4-DIN tool steel, hardened and tempered to 60 HRc.

The tool path was generated with the commercial software MasterCAM using the options available for spherical ball nose end mills (e.g. software compensation) and consisted of helical trajectories with a feed rate of 1000 mm/min and a downward feed size of 0.2 mm per revolution. The rotation of the tool was free and the lubricant applied between the tool and the blank was the forming fluid Castrol Iloform TDN81. Table 2 summarizes the experimental work plan.

Results and discussion

Pre-cut hole geometry

Table 3 summarizes the results of attempting to produce square flanges with round corners by multistage SPIF using AA1050-H111 blanks with different pre-cut geometries. In order to facilitate the analysis, it was decided to break down the initial geometry of the pre-cut holes into the individual influences of the initial side length L_0 and corner radii R_0.

Considering, for example, the influence of the initial side length L_0 of the pre-cut hole on the overall formability of the process, one may conclude that it is not possible to fabricate a square flange with a side length $L = 170$ mm and round corners from blanks with $L_0 < 136$ mm due to the occurrence of failure. On the other hand, the experimental results included in Table 3 also indicate that formability increases as the initial corner radius R_0 of the pre-cut holes increases. In fact, the maximum admissible angle attained in multistage SPIF of a square flange with round corners produced from a pre-cut hole with $L_0 = 136$ mm was found to decrease from $\Psi_6 = 90^\circ$ when $R_0 = 31.5$ mm (where vertical wall flanges are

Table 2. Work plan for investigating the production of square flanges with round corners by multistage SPIF.

Pre-cut hole		Multistage SPIF					
		Drawing angle of the intermediate stages, ψ_i(°)					
Side length, L_0 (mm)	Corner radius, R_0 (mm)	1st	2nd	3rd	4th	5th	6th
126	5, 10, 22.5, 31.5	65	70	75	80	85	90
136							
140							
147							
154							

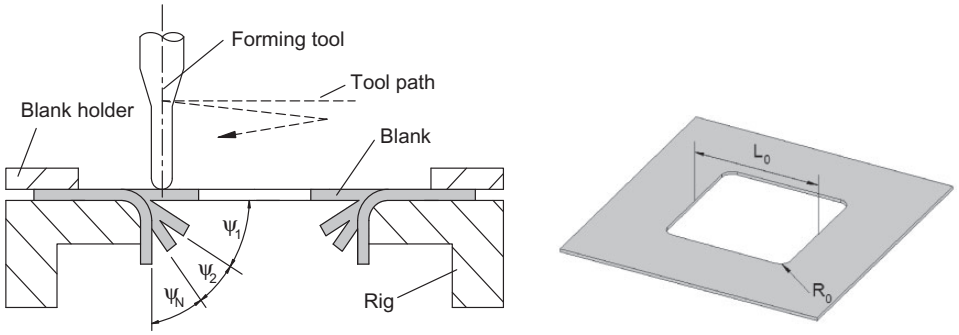

SPIF: single point incremental forming.

Table 3. Summary of the results obtained for square flanges with round corners produced by SPIF. Light and dark grey cells correspond to successful and unsuccessful results, respectively.

		Multistage SPIF					
		Drawing angle of the intermediate stages, ψ_i (°)					
L_0 (mm)	R_0 (mm)	65	70	75	80	85	90
126	5						
136							
140							
147							
154							
126	10						
136							
140							
147							
154							
126	22.5						
136							
140							
147							
154							
126	31.5						
136							
140							
147							
154							

SPIF: single point incremental forming.

successfully formed) to values of $\Psi_4 = 80°$ when $R_0 = 22.5$ mm and $\Psi_1 < 65°$ when $R_0 \leqslant 10$ mm. In the last two cases no vertical wall flanges are allowed to be formed.

The reduction in formability (and, therefore, in the maximum admissible drawing angle ψ_i,) derived from diminishing the side length L_0 and the corner radius R_0 is primarily attributed to the reduction of the initial area $A_0 = L_0^2 - R_0^2(4 - \pi)$ of the pre-cut holes. This is because small pre-cut holes, experiencing little or no expansion at all (like in case of $L_0 = 126$ mm and $R_0 = 5$ mm), are responsible for approaching plastic flow to that of conventional SPIF of a rectangular pyramid, which fails by cracking at $\Psi_{max} < 75°$ (for a reduction in thickness $t_{red} = 74\%$) according to previous experiments performed by Silva et al.[11]

However, the independent influences of the side length L_0 and corner radius R_0 in the overall formability of the process is better understood by tracking the strain values of selected grid points (“A” to “U”) placed along different meridional sections of the workpiece (aa′ to dd′) at several intermediate stages of deformation ($\Psi_i = 65°$ to 90°). The tracking procedure is schematically illustrated in Figure 3 and the results are analyzed in the following sections of the paper.

Deformation mechanics

At first glance, the fabrication of square flanges with round corners may suggest that identical forming

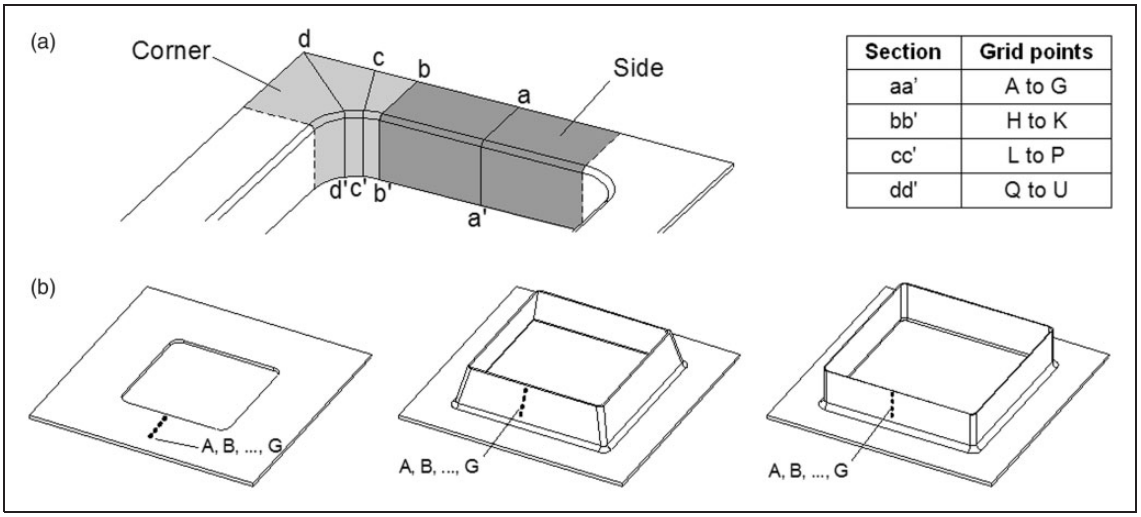

Figure 3. Breaking down the square flange with round corners into different regions for tracking the experimental in-plane strains during multistage SPIF: (a) schematic representation of four different types of meridional sections aa′, bb′, cc′, and dd′ located at the middle of the side, at the transition between the side and the corner, at the corner, and at the middle of the corner; (b) schematic representation of the selected grid points A to G placed along the meridional section that is located at the middle of the side during the initial, intermediate, and final stages of SPIF.

conditions are present to those met with during cylindrical hole-flanging produced by SPIF.[5] However, as shown in Figure 3(a), each corner (refer to the light grey area) resembles a quarter of a cylindrical flange with a very small radius and each side (refer to the dark grey area) is similar to a straight flange produced by incremental bending as the blank is turned down over the radius.

In practice, however, plastic flow is dual (or combined) due to the interaction of corners on the sides and vice versa. When the round corners of the square flanges are sufficiently large the interaction is restricted to the meridional sections bb′ and cc′ located between the most outward sections corresponding to the middle of the corners (dd′) and to the middle of the sides (aa′). The local nature of plastic deformation in SPIF accentuates the differences in deformation mechanics along sections aa′ to dd′, as shown in Figure 4.

Figure 4 is built by tracing the strain paths of the selected grid points "A" to "U" corresponding to different meridional sections (aa′ to dd′) at each intermediate stage of deformation ($\Psi_i = 65^\circ$ to 90°) that is listed in Table 2.

In case of section aa′ located at the middle of the side, the strain paths of the grid points A to G (refer to Figure 3(b)) at the six intermediate drawing angles ($\Psi_i = 65^\circ$ to 90°) are plotted as vertical lines under plane strain conditions (Figure 4(a)). Grid point D placed between the corner radius and the hole edge experiences the highest strain but its overall reduction in thickness $t_{red} = 27\%$ is far below the limiting conditions of failure provided by the FFL under plane strain conditions.

The strain paths of the grid points located at the middle of the corner (section dd′) experience plastic flow as one should a priori have expected (Figure 4(d)). In fact, all grid points exhibit linear strain paths (refer to the lines-of-best-fit through experimental data) radiating from the origin towards biaxial strain conditions. The maximum strain occurs at point R located 4 mm away from the corner radius in the undeformed blank and corresponds to a thickness reduction $t_{red} = 52\%$. The black solid curve included in Figure 4(d) is the envelope of the greatest achievable strains resulting from the strain paths of all the grid points belonging to this section. This curve results from the deformation history of selected grid points along the considered section and will be hereafter referred to as "the strain envelope" of section dd′ because each section has its own strain envelope.

From what was said above it is possible to conclude that interaction of corners on the sides and vice versa along meridional sections aa′ and dd′ is negligible in case of a square flange with round corners produced by SPIF from a blank with a pre-cut hole geometry determined by $L_0 = 140$ mm and $R_0 = 22.5$ mm.

On the contrary, the strain envelopes of the grid points belonging to sections bb′ and cc′ confirm a significant interaction between corners and sides. For example, the strain envelope of section cc′ (Figure 4(c)) is similar to that previously observed by Montanari et al.[6] in hole-flanging of cylinder flanges with large radius produced by SPIF, because the largest strain value (corresponding to $t_{red} = 61\%$) is located at the middle of the wall undergoing near plane strain conditions and the smallest strain is

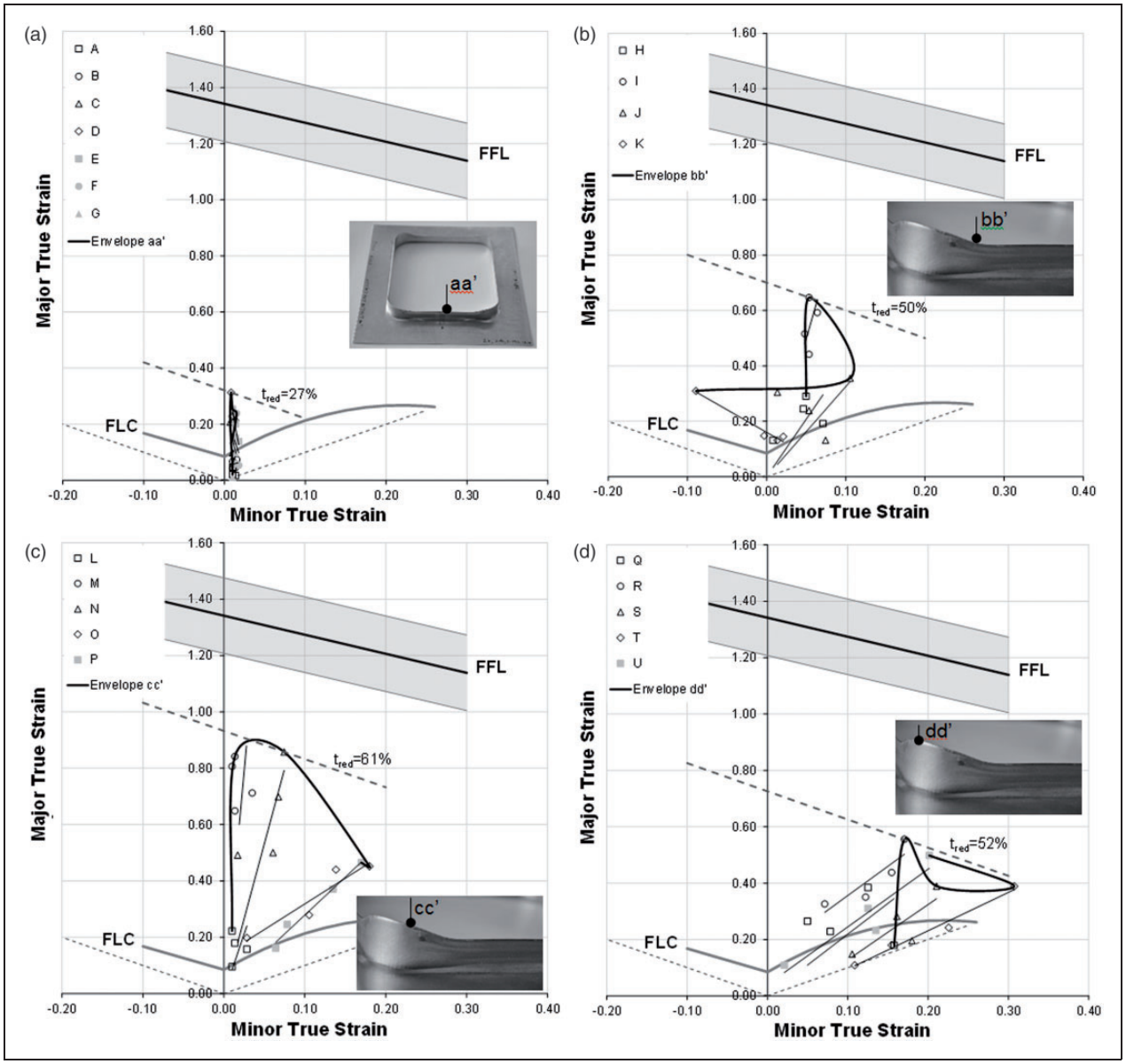

Figure 4. Deformation history of the grid points A to U located along different meridional sections (a) aa′, (b) bb′, (c) cc′ and (d) dd′ of a square flange with round corners produced by SPIF from a blank with a side length $L_0 = 140$ mm and a corner radius $R_0 = 22.5$ mm at the drawing angles $\Psi_i = 65^\circ$ to 90°. The black solid curves are the strain envelopes and the dashed grey lines are the maximum iso-thickness reduction (%) in each meridional section.
FFL: fracture forming line; FLC: forming limit curve.

located at the hole edge under biaxial stretching conditions. As a result of this, the deformation mechanics of section cc′ may be seen as a combination of two different plastic flow mechanisms; the lower part of the flange wall is primarily influenced by the side (and behaves as a straight flange) whereas the upper part of the flange wall follows the deformation mechanics of the middle section of the corner (section dd′).

However, the most interesting strain envelope is that of section bb′ (Figure 4(b)). This is because it combines biaxial strain paths that are likely to develop in the corners with radically different, nonlinear, strain paths at the hole edge that evolve from near plane strain conditions into uniaxial tension as deformation progresses. The following section explains the key role of these nonlinear strain paths in failure.

Failure

Figure 5 provides insight into the physics behind the occurrence of failure when attempting to produce a square flange from a blank with a small area A_0 of the pre-cut hole. The selected test case with $L_0 = 147$ mm and $R_0 = 5$ mm fails by tearing in the corner of the flange. The crack starts out at the edge and moves down towards the bottom corner (Figure 5(b)) and is attributed to lack of material in the corners due to incorrect (small) size of the pre-cut hole.

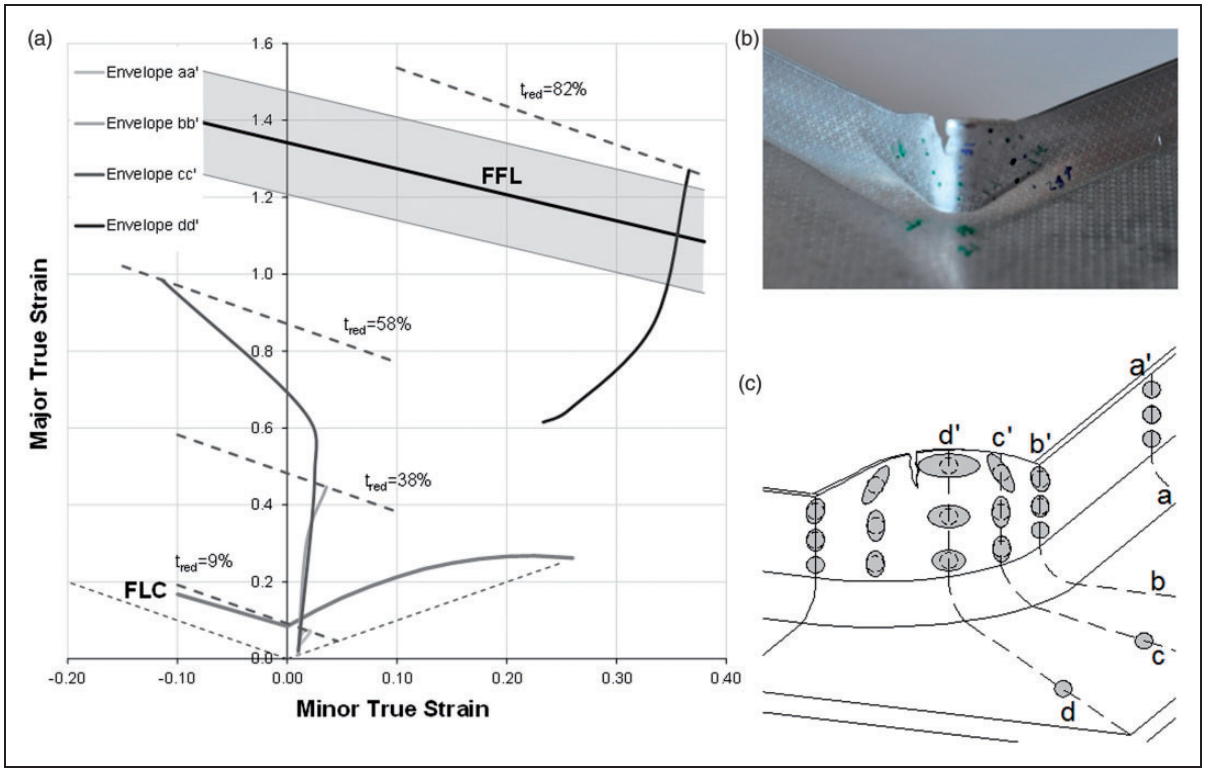

Figure 5. Deformation history of a square flange with round corners produced by SPIF from a blank with a side length $L_0 = 147$ mm and a corner radius $R_0 = 5$ mm at drawing angles $_i = 65^\circ$ to 80°: (a) strain envelopes of the grid points located along the meridional direction of sections aa′, bb′, cc′, and dd′; (b) photograph showing failure by tearing in the corner; (c) schematic representation of the deformed circles of the grid at the corner of the square flange where failure took place.
FFL: fracture forming line; FLC: forming limit curve.

The strain envelopes plotted in Figure 5(a) combined with the schematic representation of the deformed circle grid include in Figure 5(c) shows progressive rotation of the deformed circles from near plane strain to uniaxial tension as the grid points move along section cc′ towards the hole edge. This result combined with biaxial stretching conditions that are available at the middle of the corner (section dd′) produces a significant rise of the strain envelope of section dd' so that highest strains cross the FFL and lead to failure by fracture.

The morphology of the crack shown in Figure 5(b) and its propagation path along the meridional direction allows concluding that failure is triggered after exceeding the maximum load-carrying capacity due to the circumferential stresses acting on the corner of the flange. Failure is cause by a significant amount of sheet thinning until fracture (corresponding to a thickness reduction $t_{red} = 82\%$), without signs of previous localized necking.

The corrective action to solve this problem is to change the size of the pre-cut hole by increasing the side length L_0, the corner radius R_0 or both simultaneously. Table 3 provides the process formability window as a function of the geometric features of the pre-cut holes.

Conclusions

The deformation mechanics of square flanges with round corners produced by SPIF was associated with four different regions: (i) the sides undergoing plane strain conditions, (ii) the middle of the corners experiencing biaxial strain conditions and the regions located (iii) at the transition between the sides and the corners and (iv) at the corners, which experience more complex strain paths due to the interaction between the middle of the corners and the sides.

The strain envelopes of the grid points located at the transition between the sides and the corners are similar to those recently observed by the authors in hole-flanging of cylindrical hole-flanges with large radius produced by SPIF. The strain envelopes of the grid points located in-between the middle of the corners and the transition between the sides and the corners experience nonlinear strain paths that evolve from near plane strain conditions into uniaxial tension as deformation progresses.

Crack morphology and propagation paths starting out at the edges and moving down along the meridional direction towards the bottom corners, allows concluding that failure is triggered after exceeding the maximum load-carrying capacity due

to circumferential stresses. Failure is caused by sheet thinning until fracture without signs of previous localized necking and may be prevented by changing the geometry of the pre-cut hole by increasing the side length L_0, the corner radius R_0 or both simultaneously.

Acknowledgement

The work of André Teodora and Pedro Pardal is greatly acknowledged.

Funding

The work was partially supported by the Portuguese Foundation for Science and Technology under the research contract PEst-OE/EME/LA0022/2011. Luciana Montanari would like also to acknowledge FAPESP (Fundação de Amparo à Pesquisa do Estado de São Paulo) for the financial support.

References

1. Jeswiet J, Micari F, Hirt G, et al. Asymmetric single point incremental forming of sheet metal. *Ann CIRP* 2005; 54: 623–650.
2. Nimbalkar DH and Nandedkar VM. Review of incremental forming of sheet metal components. *Int J Eng Res Appl* 2013; 3: 39–51.
3. Cui Z and Gao L. Studies on hole-flanging process using multistage incremental forming. *CIRP J Manuf Sci Technol* 2010; 2: 124–128.
4. Petek A, Kuzman K and Fijavž R. Backward drawing of necks using incremental approach. *Key Eng Mater* 2011; 473: 105–112.
5. Centeno G, Silva MB, Cristino V, et al. Hole-flanging by incremental sheet forming. *Int J Mach Tools Manuf* 2012; 59: 46–54.
6. Montanari L, Cristino VA, Silva MB, et al. A new approach for deformation history of material elements in hole-flanging produced by single point incremental forming. *Int J Adv Manuf Technol*. DOI: 10.1007/s00170-013-5117-4.
7. Silva MB, Martinho TM and Martins PAF. Incremental forming of hole flanges in polymer sheets. *Mater Manuf Process* 2013; 28: 330–335.
8. Voswinckel H, Bambach M and Hirt G. Process limits of stretch and shrink flanging by incremental sheet metal forming. *Key Eng Mater* 2013; 549: 45–52.
9. Atkins AG. Fracture in forming. *J Mater Process Technol* 1996; 56: 609–618.
10. Silva MB, Teixeira P, Reis A, et al. On the formability of hole-flanging by incremental sheet forming. *J Mater Des Appl* 2013; 227: 91–99.
11. Silva MB, Nielsen PS, Bay N, et al. Failure mechanisms in single point incremental forming of metals. *Int J Adv Manuf Technol* 2011; 56: 893–903.
12. Hirt G, Ames J, Bambach M, et al. Forming strategies and process modelling for CNC incremental sheet forming. *CIRP Ann Manuf Technol* 2004; 53: 203–206.